

# **Antibacterial Liquid Metals: Biofilm Treatment *via* Magnetic Activation**

Aaron Elbourne,<sup>1,2,#</sup> Samuel Cheeseman,<sup>1,2,#</sup> Paul Atkin,<sup>3,4</sup> Nghia P. Truong,<sup>5</sup> Nitu Syed,<sup>3</sup> Ali Zavabeti,<sup>3</sup> Md Mohiuddin,<sup>3</sup> Dorna Esrafilzadeh,<sup>3,6</sup> Daniel Cozzolino,<sup>1</sup> Chris F. McConville,<sup>1</sup> Michael D. Dickey,<sup>7</sup> Russell J. Crawford,<sup>1,2</sup> Kourosh Kalantar-Zadeh,<sup>8</sup> James Chapman,<sup>1,2,\*</sup> Torben Daeneke,<sup>3,\*</sup> Vi Khanh Truong<sup>1,2,\*</sup>

<sup>1</sup>School of Science, College of Science, Engineering and Health, RMIT University, Melbourne VIC 3001, Australia

<sup>2</sup>Nanobiotechnology Laboratory, RMIT University, Melbourne VIC 3001, Australia

<sup>3</sup>School of Engineering, RMIT University, Melbourne, Victoria 3001, Australia

<sup>4</sup>CSIRO Australia, Private Bag 33, Clayton South MDC, Clayton, Victoria 3169, Australia

<sup>5</sup>ARC Centre of Excellence in Convergent Bio-Nano Science and Technology, Monash Institute of Pharmaceutical Sciences, Monash University, 399 Royal Parade, Parkville, Victoria 3152, Australia

<sup>6</sup>Graduate School of Biomedical Engineering, University of New South Wales, Sydney, NSW 2052, Australia

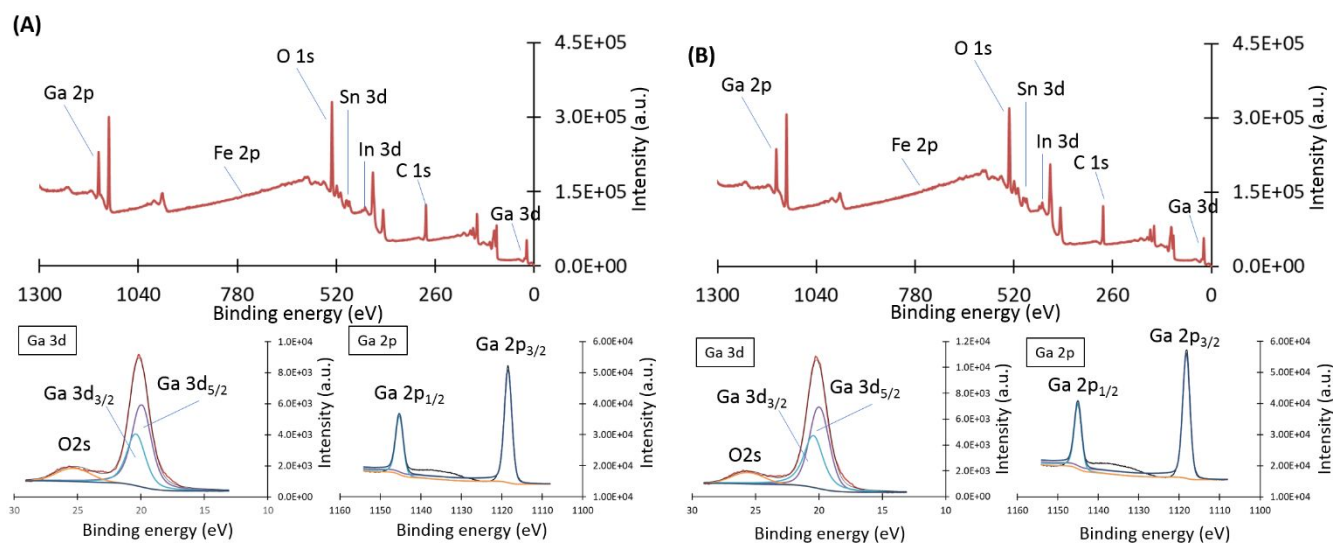
<sup>7</sup>Department of Chemical and Biomolecular Engineering, North Carolina State University, Raleigh, North Carolina 27695, USA

<sup>8</sup>School of Chemical Engineering, University of New South Wales, Kensington, NSW 2052, Australia

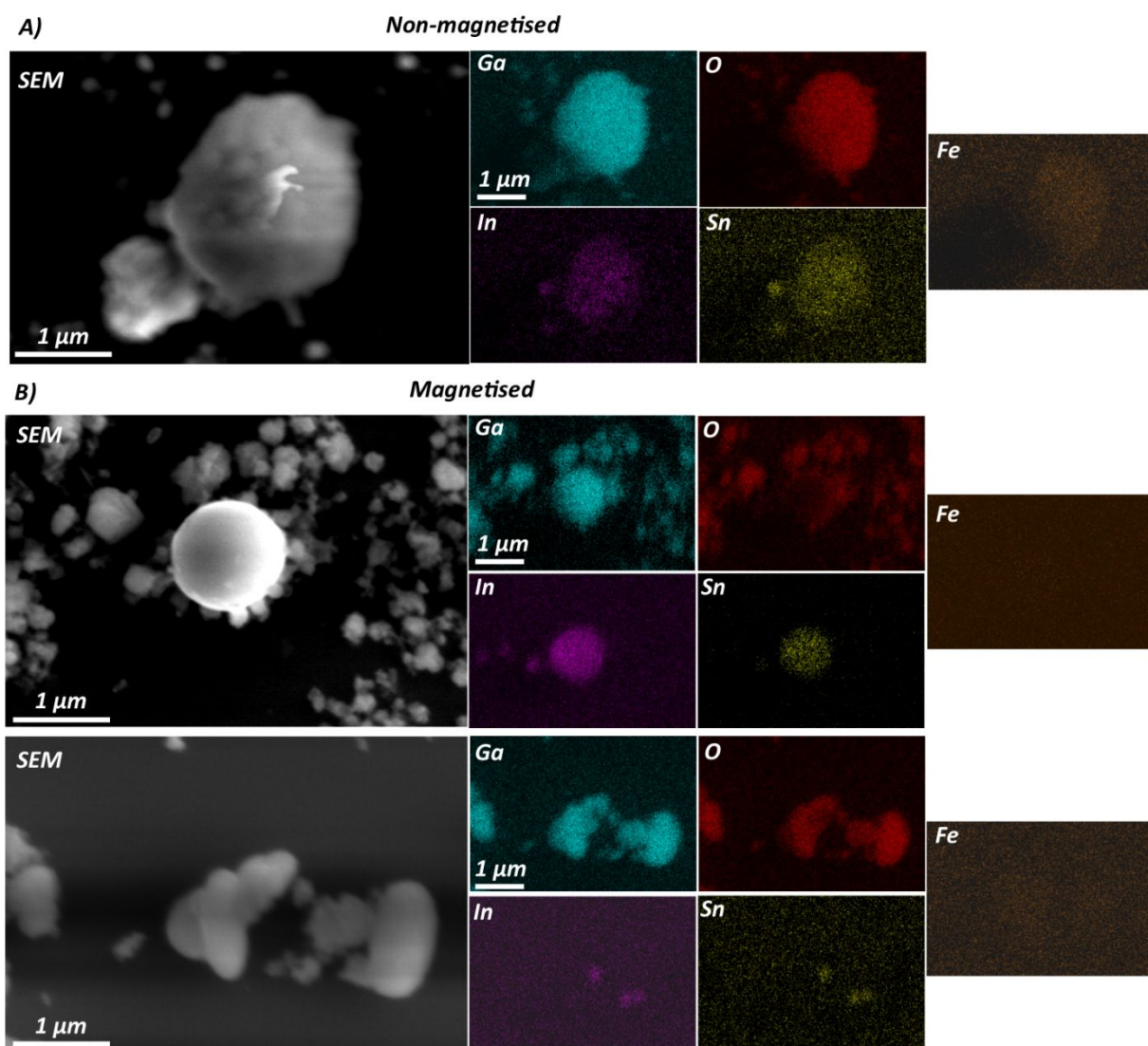
# These authors contributed equally.

\* Corresponding Authors

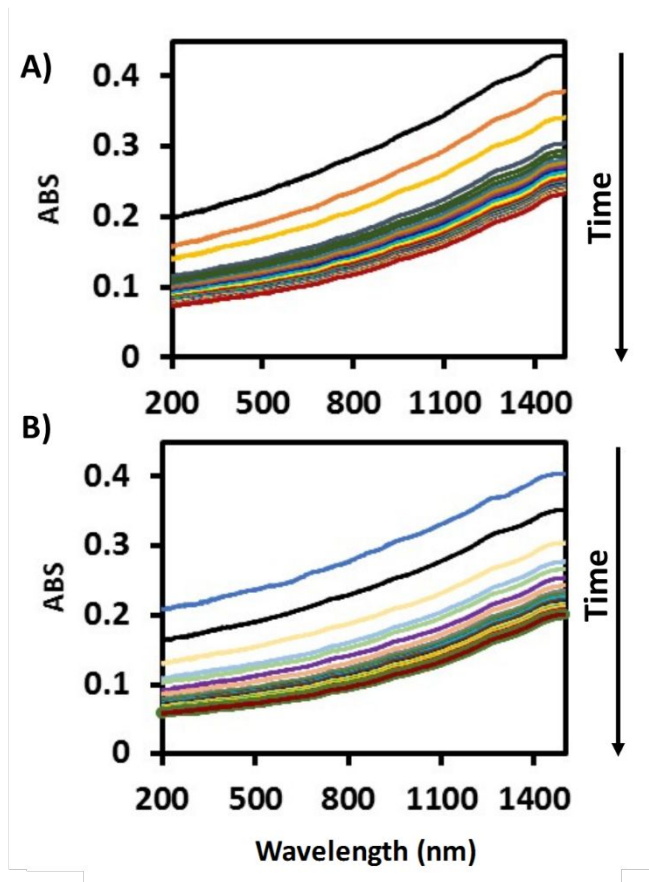
## Supporting Information



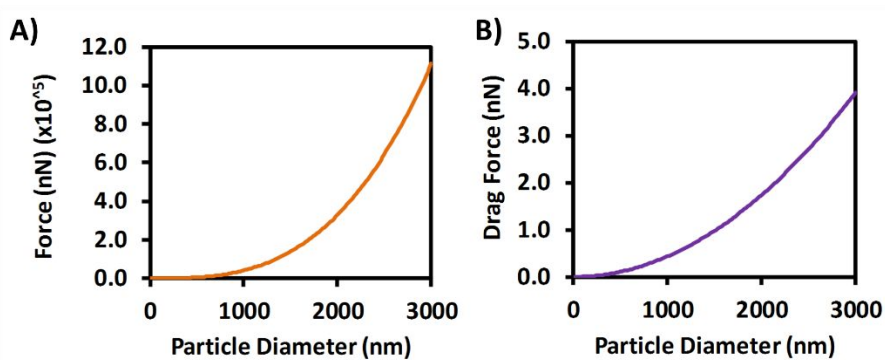
**Figure S1.** High resolution XPS spectra of the **A)** pre-magnetised and **B)** post-magnetised GLM-Fe particles drop cast onto a clean silicon substrate. Peak positions and binding energy ranges were auto selected by the Advantage software. Peaks were assigned in accordance with the Advantage database,  $\text{Ga}^0$  peaks are located at 18.7 eV (Ga 3d), 159.5 eV (Ga 3s) and 1117 eV (Ga 2p) eV.  $\text{In}^0$  and  $\text{Sn}^0$  peaks are observed at 444 eV (In 3d) and 484.8 eV (Sn 3d), respectively. Importantly, no distinct changes were observed between the pre-magnetised and post-magnetised samples. Oxygen and Carbon peaks were associated with the silicon substrate that was used as a support for the GLM-Fe particles. For the Ga 3d data, the red line is the experimental data, the black line is the general fit, the purple line is  $\text{Ga}3d_{5/2}$  (Element), the teal line  $\text{Ga}3d_{3/2}$  (Element), the teal line  $\text{Ga}3d_3$  (Native Oxide). For the Ga 2p data, the black line is the experimental data, the blue line is the general fit, the teal line is the  $\text{Ga}2p_{1/2}$  (Native Oxide).



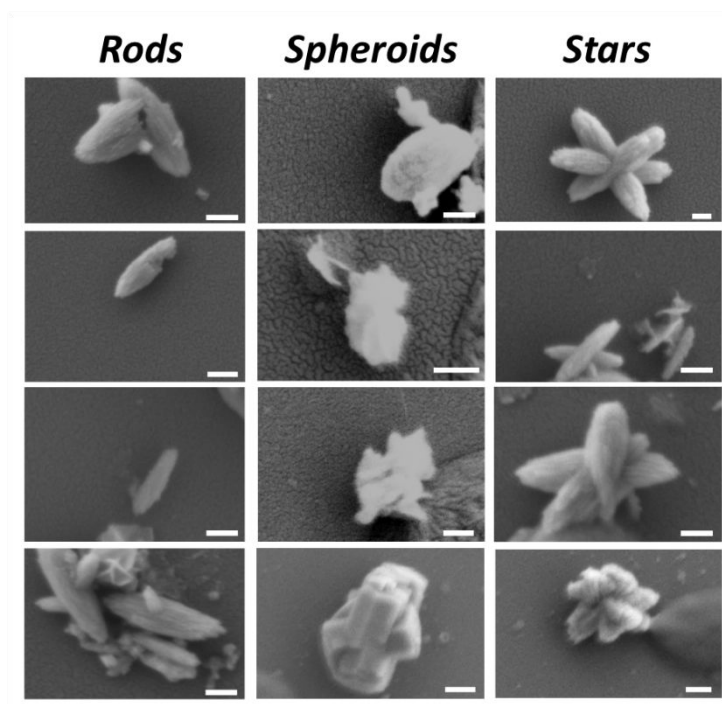
**Figure S2.** EDX spectra of the **A)** pre-magnetised and **B)** post-magnetised GLM-Fe particles drop cast onto a clean silicon substrate. The respective SEM images are shown along side the EDX maps of Gallium (Ga), Indium (In), Oxygen (O), Tin (Sn), and Iron (Fe).



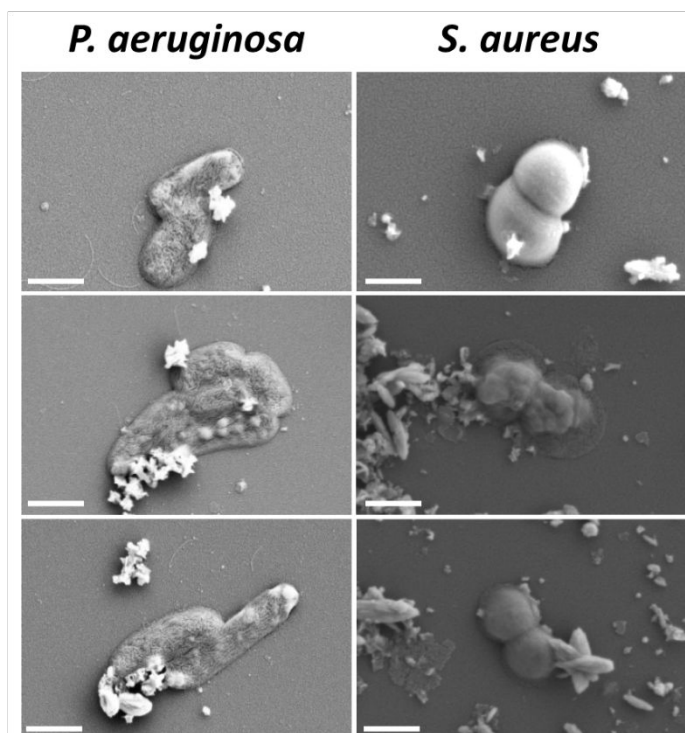
**Figure S3.** UV-vis spectra of the GLM-Fe particle solution as a function of time. The curves were obtained over a period of 24 hours at intervals of 1 hour. **A)** Shows the initial solution following fabrication of sonication. **B)** Spectra obtained following initial settling and then resuspension via mechanical shaking. Importantly, this shows that the particles can be resuspended for use via shaking.



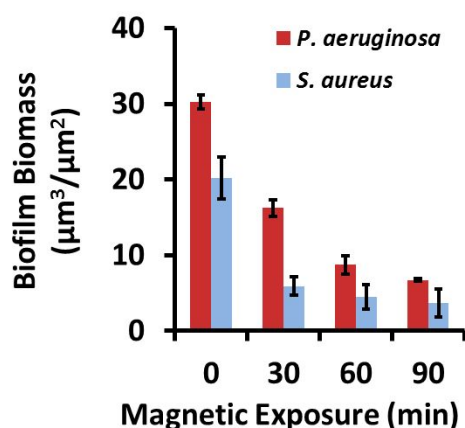
**Figure S4.** **A)** Force of particle as a function of the size of magnetic inclusion. **B)** Drag force experienced by the particle as function of particle diameter.



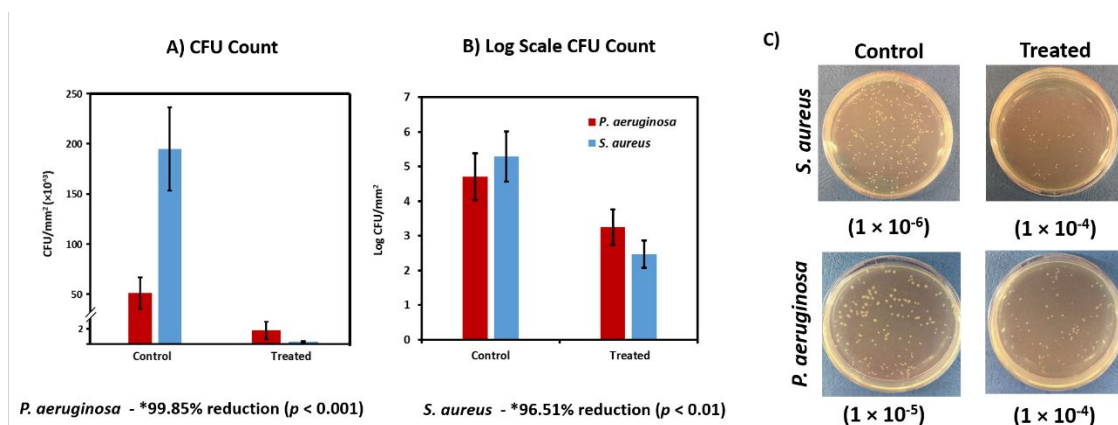
**Figure S5.** A collection of SEM micrographs displaying the variant morphologies of post-magnetised GLM-Fe particles. Importantly, the resulting particle shapes appeared to be somewhat random, meaning that the system is chaotic. The particles could largely be placed into three morphological categories, including rods, spheroids, and stars. The white scale bar is 200 nm in each image, respectively.



**Figure S6.** Additional SEM micrographs of **(left)** *P. aeruginosa* and **(right)** *S. aureus* cells following 90 minutes of exposure to the rotating magnetic fields in the presence of GLM-Fe particles. The white scale bars are 500 nm.



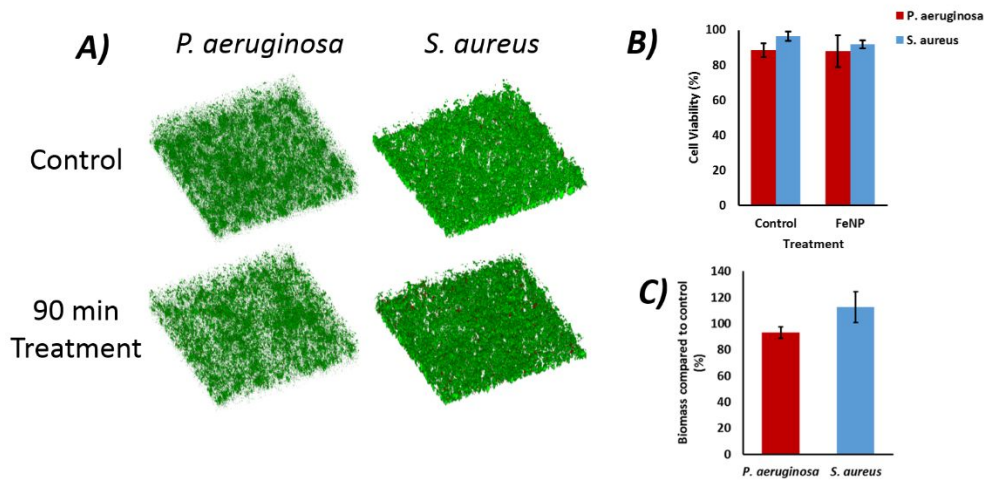
**Figure S7.** Raw biofilm mass ( $\mu\text{m}^3/\mu\text{m}^2$ ) as a function of magnetic activation. The p-values for treatment times of 30, 60, and 90 min are 0.001,  $9.03 \times 10^{-5}$ , and 0.0003 and 0.006, 0.009, and 0.014 for *P. aeruginosa* and *S. aureus*, respectively, compared to control. N = 3 for all samples.



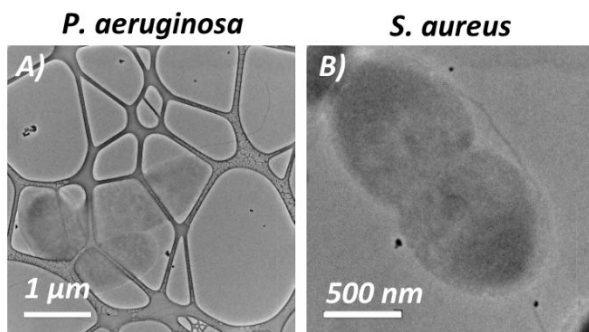
**Figure S8.** A) Raw CFU count and B) CFU count displayed on a logarithmic scale for control and treated with magnetically activated GLM-Fe particles for *P. aeruginosa* and *S. aureus* biofilms. C) Representative plates from the CFU experiments.



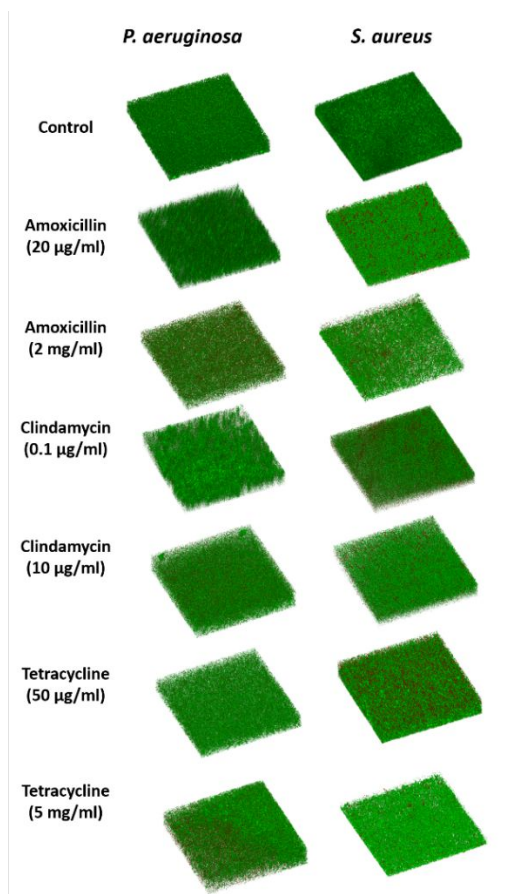
## Iron NPs



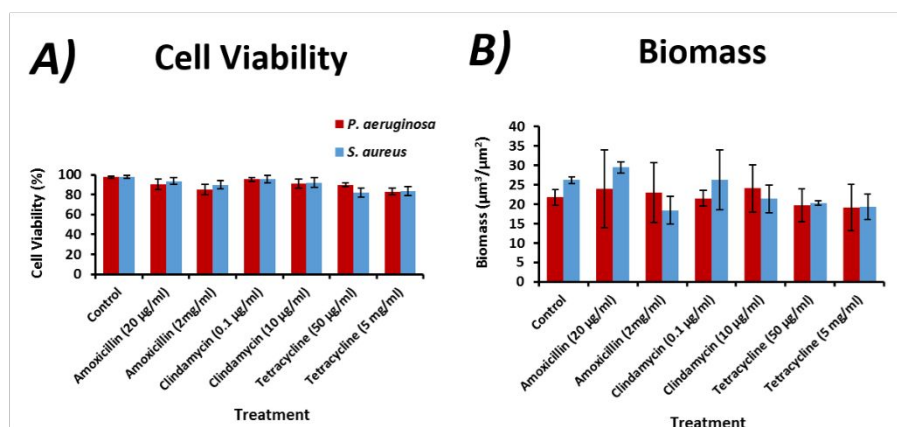
**Figure S9.** A) CLSM images of *Pseudomonas aeruginosa* (left) and *Staphylococcus aureus* (right) biofilms following 90 min magnetic exposure to iron nanoparticles (FeNP). The CLSM images are  $220\ \mu\text{m} \times 220\ \mu\text{m}$ . B) Average number of viable cells expressed as a percentage and C) Biofilm biomass following the magnetic exposure, expressed as a percentage of the control biomass. No statistical significance was noted between systems.  $N = 2$  for each system.



**Figure S10.** TEM images of bacteria co-cultured with GLM-Fe particles in the absence of magnetic field. Importantly, there is no sign of cellular damage or particles entering the cells.

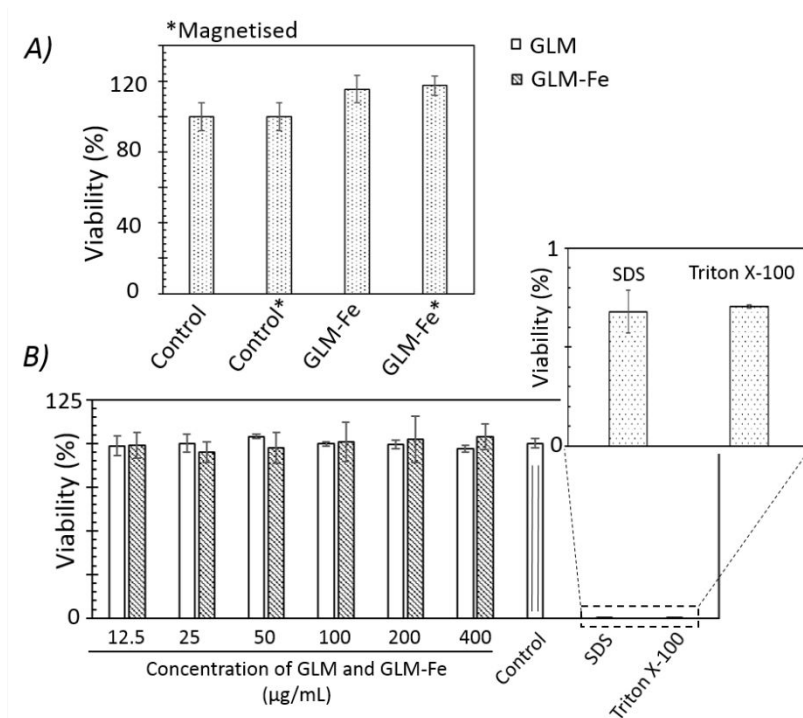


**Figure S11. Antibiotic Susceptibility of Biofilms.** Representative CLSM images of *P. aeruginosa* and *S. aureus* biofilms following 90 minutes of treatment with the antibiotics amoxicillin, clindamycin, and tetracycline at the MIC concentration and at 100× the MIC. The exact concentrations are displayed to the left of the respective images.

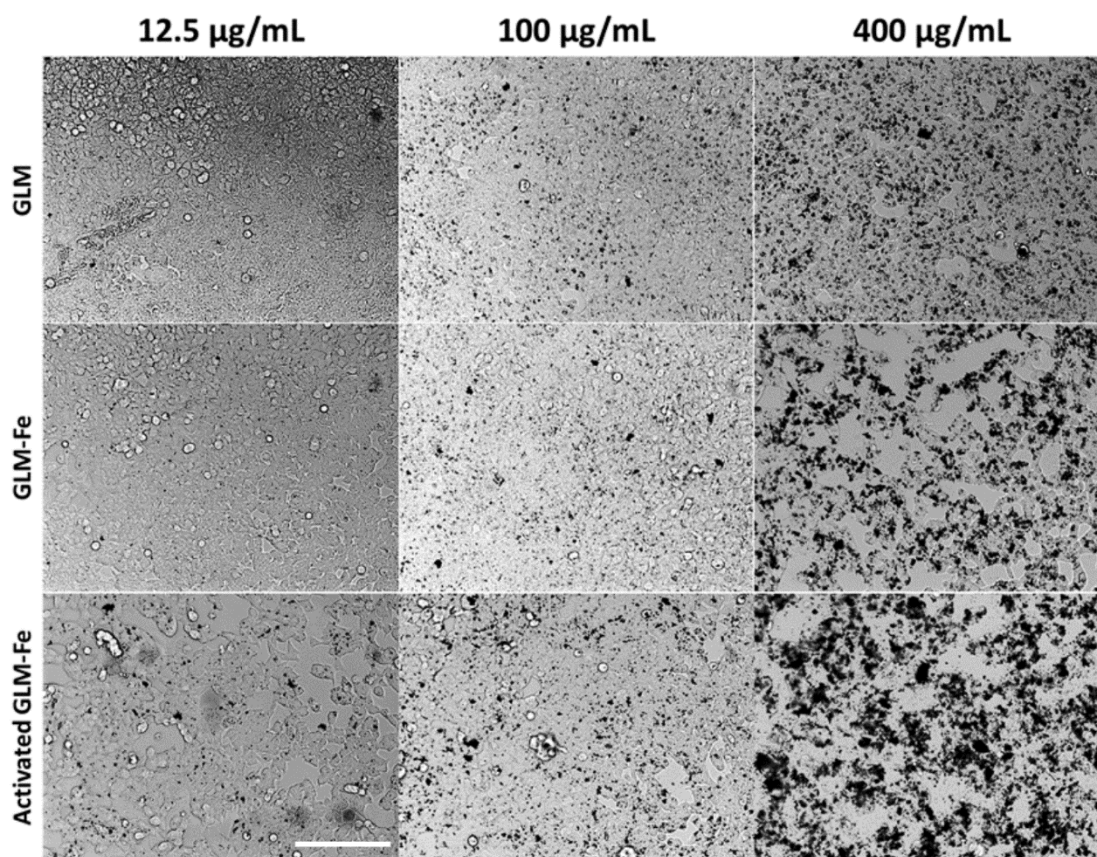


**Figure S12. A) Cell viability and B) Raw biofilm mass ( $\mu\text{m}^3/\mu\text{m}^2$ )** following treatment with the antibiotic amoxicillin, clindamycin, and tetracycline at the indicated concentrations. No statistical significance was noted between systems.  $N = 2$  for each system.





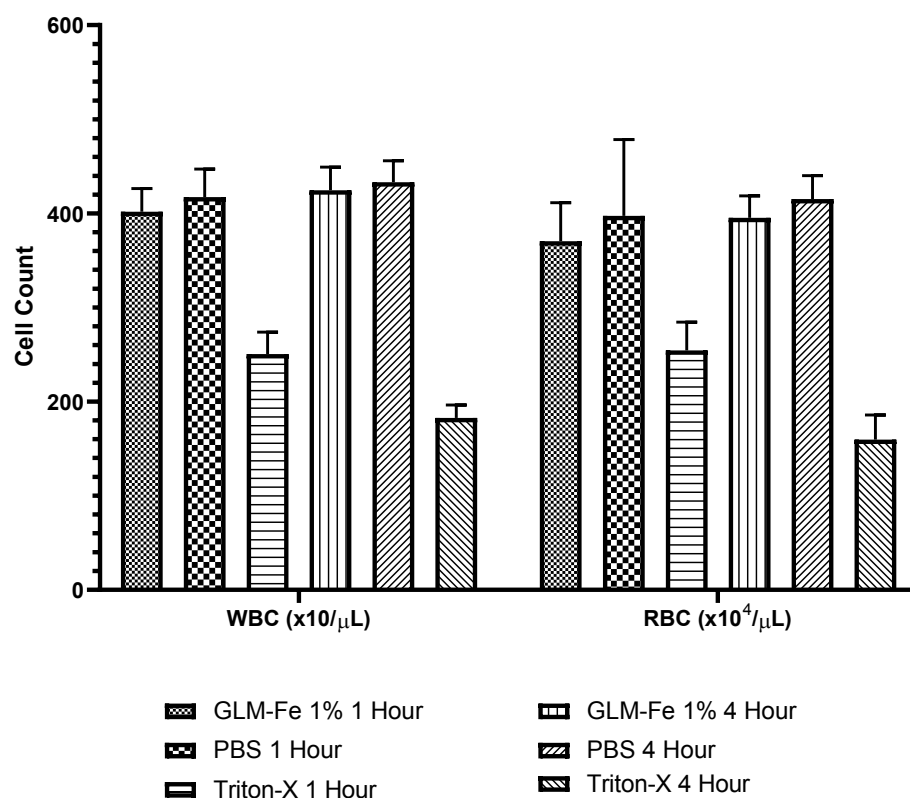
**Figure S13.** Assessment of cytotoxicity of the galinstan (GLM), galinstan-Fe (GLM-Fe), and magnetically activated GLM-Fe particles on HEK cell lines. **A)** The data shows the viability of HEK cells in the presence of particles (100 µg/mL) after 2 days of incubation against control samples (with no introduction of particles) with and without magnetisation for 90 minutes. **B)** Assessment of the innate cytotoxicity of the galinstan (GLM) and galinstan-Fe (GLM-Fe) particles without magnetisation as a function of concentration. The negative control is cells grown without the presence of any particles, and the positive control SDS and Triton X-100 (0.1 wt%/vol) were included to show the efficacy of the AlamarBlue assay. These data were compared with the untreated HEK cells and expressed in terms of the cell viability (%). Each experiment was repeated three times.



**Figure S14.** Optical phase contrast images showing no inhibition of HEK cell growth after treatment with galinstan, GLM-Fe and activated GLM-Fe. Interestingly, despite the increase in the concentration of materials, HEK cells were shown to be able to proliferation and differentiation. Under the activation of magnetic field, HEK cells seem to grow healthily after 2 day incubation. The white scale bar (bottom left) is 100  $\mu\text{m}$ .

### **Red Blood Cell and White Blood Cell Lysis**

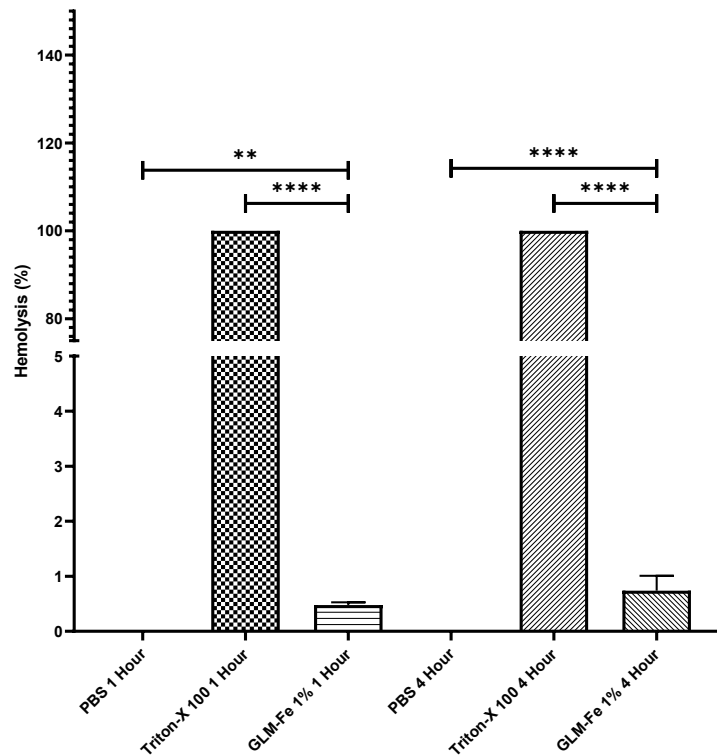
Quantitative results are needed to ensure the hemocompatibility of the particle used. White blood cells (WBC) and red blood cells (RBC) count was observed using automated blood parameters analyser Sysmex X1000i. Samples were incubated in shaking incubator at 37C to mimic the condition of the moving blood in the body. From the results obtained from the analysis (Figure S9), indicate that there is no statistically significant difference ( $P>0.05$ ) between GLM-Fe samples with PBS either in WBC and RBC count. However, there are significant differences between all groups of GLM-Fe and PBS with Triton-X. This indicates that the exposure of GLM-Fe does not induce any significant changes in the amount of WBC and RBC. There was also no difference in the results from groups of different hours, which demonstrate that Lysis occurs almost instantly in Triton-X 100%.



**Figure S15.** Sysmex X1000i result of white blood cell (WBC) and red blood cell (RBC) content with 1 and 4 hour of incubation time

### **Haemolysis Percentage**

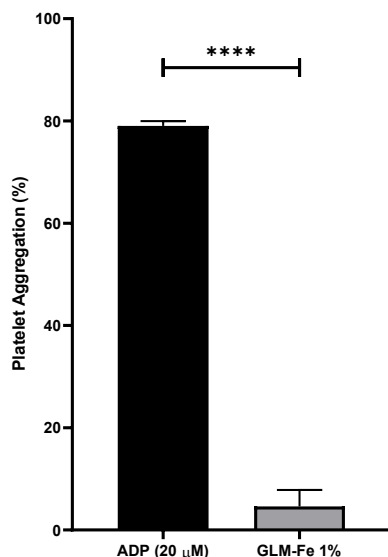
Haemolysis percentage was also observed by incubating washed red blood cells in samples and the percentage was calculated by comparison with totally lysed sample (Triton-X 100) and negative control which produces no lysis (PBS). As shown in Figure S10, GLM-Fe had minimal effect towards the red blood cell lysis. Haemolysis percentage below 2% is considered non-haemolytic which indicate that GLM-Fe particles did not induce haemolysis.<sup>1</sup>



**Figure S16.** Percent of haemolysis observed in samples. Triton-X groups were significantly different with all the other groups ( $P < 0.0001$ ).

### **Platelet Aggregation**

To observe the effect of GLM-Fe towards platelet aggregation, GLM-Fe samples were incubated in platelet rich plasma and compared with ADP a known platelet aggregation activator as a positive control. For platelet aggregation a threshold of 20% was known as the limit and as observed in Figure S11, GLM-Fe did not induce significant platelet aggregation with percentage of platelet aggregation below threshold (2).



**Figure S17.** Platelet aggregation of GLM-Fe compared with ADP.

## **METHODOLOGY**

### *Red Blood Cells and White Blood Cells Lysis*

In order to analyse the effect of liquid metal on red blood cells and white blood cells count human blood from healthy volunteers was collected in citrated vacutainer. To a volume of 600  $\mu$ L of whole blood, 60  $\mu$ L of sample was added and incubated in a shaking incubator at 37°C for 1 and 4 hours. After incubation, 20  $\mu$ L of the sample was added with 140  $\mu$ L of CellPack® buffer to ensure a ratio of 1:7. The samples were then analysed using Sysmex® X1000i to observe the blood parameters. Triton-X 100 1% was used as a positive control to ensure lysis of cells, while PBS was used as the negative control.

### *Haemolysis Percentage*

Blood was centrifuged at 1000 rpm for 15 minutes to separate plasma with red blood cells. The red blood cells were obtained by separating the plasma and followed by washing of the red blood cells twice with PBS. A stock of red blood cells was created by diluting 1 mL of washed red blood cells into a final volume of 50 ml with PBS. As much as 20  $\mu$ L of liquid metal sample was placed in a well of a 96 well plate and 180  $\mu$ L of the red blood cells stock solution was added. Triton-X 100 1% and PBS were used as positive and negative control respectively. The plate was then placed in a shaking incubator at 37°C for 1 and 4 hours. After incubation, the plate was then centrifuged at 1000 rpm for 5 minutes and aspirate the supernatant to transfer to a different well plate for reading. The samples were then observed for absorbance using a plate reader at 545 nm. Percent haemolysis was calculated using the equation below (Eq.2).

$$\text{Haemolysis (\%)} = \frac{\text{Absorbance sample} - \text{Absorbance negative control}}{\text{Absorbance positive control} - \text{Absorbance negative control}} \times 100 \quad (\text{Eq.2})$$

### Platelet Aggregation

Platelet rich plasma (PRP) was obtained from blood of healthy volunteers by centrifugation at 1000 rpm for 15 minutes. After centrifugation, plasma was then separated from the red blood cells and placed in a clean tube. In a tube, 20  $\mu\text{L}$  of samples were added with 100  $\mu\text{L}$  of PRP and incubated for 1 hour in a shaking incubator at 37°C. The platelet count (PC) were then analysed using Sysmex X1000i. Adenosine diphosphate (ADP) was used as a positive control and DPBS (PBS without  $\text{Ca}^{2+}$  or  $\text{Mg}^{2+}$ ) as a negative control. The percentage of platelet aggregation was analysed by using equation shown in Eq.3.

$$\text{Platelet aggregation (\%)} = \frac{\text{PC negative control} - \text{PC sample}}{\text{PC negative control}} \times 100\% \quad (\text{Eq.3})$$

### Statistical Analysis

All of the statistical analysis was calculated by one-way analysis of variance (ANOVA) using GraphPad Prism 8 software.

**Table S1.** Comparison of passive antibacterial nanomaterials.

Materials	Sizes/Thickness	Concentration	Bacterium	Efficacy	Biofilm Eradication	Treatment time
<b>Ag<sup>3</sup></b>	4 nm - 24 nm	50 $\mu\text{g/ml}$	<i>Escherichia coli</i>	100%	N	24 hour incubation with bacteria
<b>Au<sup>4</sup></b>	10 nm - 200 nm	Widely Variant	Various	NB	N	N/A
<b>ZnO<sup>5</sup></b>	249 nm	0.25 g/L (0.25 mg/mL)	<i>Escherichia coli</i>	80% growth reduction	N	2 hour to be effective against bacteria
<b>Graphene oxide<sup>6</sup></b>	0.31 $\mu\text{m} \pm 0.20 \mu\text{m}$	80 $\mu\text{g/mL}$	<i>Escherichia coli</i>	90%	N	2 hour to be effective against



						bacteria
<b>Reduced graphene oxide<sup>6</sup></b>	2.75 $\mu\text{m} \pm 1.18 \mu\text{m}$	80 $\mu\text{g/mL}$	<i>Escherichia coli</i>	80%	N	2 hour to be effective against bacteria

N:no, NB: Not bactericidal, N/A: not applicable

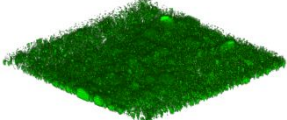
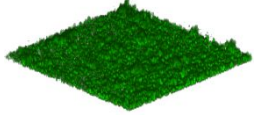
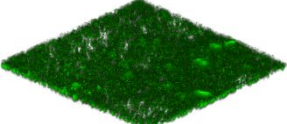
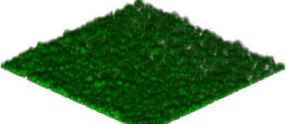
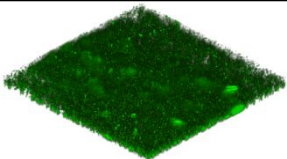
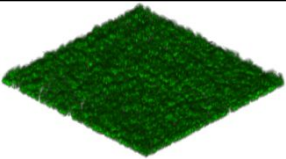


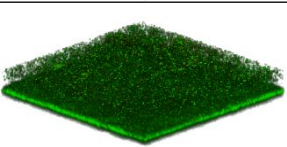
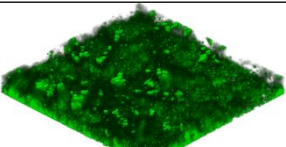

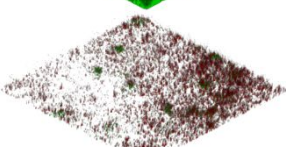
**Table S2.** Comparison of stimuli responsive (activated) antibacterial nanomaterials.

Materials	Sizes/Thickness	Activator	Concentration	Bacterium	Efficacy	Biofilm Eradication	Treatment Time
<b>ZnO nanoparticles<sup>7</sup></b>	60 nm	UV-visible Light	Embedded in PDMS and photosensitizer crystal violet (50 mg/g)	<i>Escherichia coli</i> <i>Staphylococcus aureus</i>	4 log reduction  95% reduction	N	N/A
<b>ZnO nanoparticles<sup>5</sup></b>	50 – 70 nm	UV-visible Light	10 mM	<i>Staphylococcus aureus</i> <i>Staphylococcus epidermidis</i>	More than 90% reduction	N	N/A
<b>TiO<sub>2</sub> nanoparticles<sup>8</sup></b>	79 nm	UV-visible Light	1200 $\mu\text{M}$	<i>Escherichia coli</i>	75% reduction	N	N/A
<b>Cu-TiO<sub>2</sub> nanoparticles<sup>9</sup></b>	15-50 nm	UV-visible Light	Drop-casting 1 mg/mL nanoparticle suspension onto the 2 cm $\times$ 2 cm glass substrate	<i>Escherichia coli</i>	100% reduction	N	N/A

<b>V<sub>2</sub>O<sub>5</sub> nanowires</b> 10	average length of 300 nm and a width of 20 nm	uv-visible Light	0.075 mg ml <sup>-1</sup>	<i>Escherichia coli</i> <i>Staphylococcus aureus</i>	Inhibit the growth of bacteria	I	180 minutes to inhibit the growth of bacteria
<b>Gold nanostar</b> 1	50 – 100 nm	NIR laser	Monolayer of nanostar on glass	<i>Staphylococcus aureus</i>	99%	I	30 minutes to eradicate the monolayer of bacteria
<b>Gold nanocross</b> 12	~100 nm	NIR laser	0.2 mg/mL	<i>Pseudomonas aeruginosa</i>	99%	I	5 minutes to eradicate the monolayer of bacteria
<b>Fe-Galinstan particles (This Study)</b>	nm - μm (wide variation)	Rotating magnetic field	0.1 mg/mL	<i>Pseudomonas aeruginosa</i> <i>Staphylococcus aureus</i>	99% Inactivation	D	90 minutes to eradicate the 25 μm-thick biofilm

N:no, I: Inhibition, D: Disintegration

**Table S3.** Table 1 recreated with the respective CLSM image of the active biofilm. All 3D plots represent a 220  $\mu\text{m}$   $\times$  220  $\mu\text{m}$  area.

Material	Condition	Biofilm Degradation	Antibacterial Behaviour	Biofilm CLSM Images	
				<i>P. aeruginosa</i>	<i>S. aureus</i>
GLM	24 Bacterial Incubation	×	×		
	90 min Magnetic Exposure	×	×		
GLM-Fe	24 Bacterial Incubation	×	×		
	90 min Magnetic Exposure	✓	✓		
Post-Magnetised GLM-Fe	24 Bacterial Incubation	×	×		
	90 min Magnetic Exposure	✓	✓		

**Table S4.** Comparative effect of last-line antibiotics on established biofilms.

Bacteria	Antibiotic	Efficacy Against Biofilm	Exposure Time	Notes
<i>S. aureus</i>	Vancomycin (2 mg/ml) <sup>13</sup>	0%	24 h	
	Tigecycline (2 mg/ml) <sup>13</sup>	85 ± 30%	24 h	
	Tigecycline (64 µg/ml) <sup>14</sup>	~65%	24 h	
<i>P. aeruginosa</i>	Imipenem (64 µg/ml)* <sup>15</sup>	Log 3 increase	12 h	<i>In Vivo</i> study
	Colistin (256 µg/ml) <sup>15</sup>	Log 4 increase	12 h	<i>In Vivo</i> study
	Imipenem (0.5 µg/ml) <sup>16</sup>	~165% increase	37 h	
	Tigecycline <sup>17</sup>	NR: inherent Resistance	N/A	

\*Commercial name for carbapenem

**Table S5.** Comparison of Elastic Moduli of Various Bacterial and Eukaryotic Cells.

Cell Type	Species	Strain / Source	Method of Determination	Elastic Modulus
<b>Bacteria</b>	<i>Escherichia coli</i> <sup>18</sup>	NS	AFM (Force Curves)	23 ± 8 MPa - 49 ± 20 MPa
	<i>Escherichia coli</i> <sup>19</sup>	NCTC 9001	AFM (Force Curves)	221.4 ± 11.9 MPa
	<i>Pseudomonas aeruginosa</i> <sup>20</sup>	PAO1	CLAMP	100–200 MPa
	<i>Staphylococcus aureus</i> <sup>19</sup>	NCTC 8532	AFM (Force Curves)	95.4 ± 2.6 MPa
<b>Eukaryotes</b>	Cardiocytes <sup>21</sup>	Isolated from rabbits	AFM (Force Curves)	90–110 kPa
	Endothelial cells <sup>22</sup>	Harvested from bovine	AFM (Force Curves)	10–11 kPa
	Fibroblasts <sup>23</sup>	NIH3T3	AFM (Force Curves)	4 to 100 kPa
	Osteoblasts <sup>24</sup>	Patient Sourced	AFM (Force Curves)	0.3–20.0 kPa
	Red blood cells <sup>25</sup>	Patient Sourced	AFM (Force Curves)	129.56 - 149.69 kPa

## References

1. Mesdaghinia, A.; Pourpak, Z.; Naddafi, K.; Nodehi, R. N.; Alizadeh, Z.; Rezaei, S.; Mohammadi, A.; Faraji, M., An *In Vitro* Method to Evaluate Hemolysis of Human Red Blood Cells (RBCs) Treated by Airborne Particulate Matter (PM10). *MethodsX* **2019**, *6*, 156-161.
2. Huang, H.; Lai, W.; Cui, M.; Liang, L.; Lin, Y.; Fang, Q.; Liu, Y.; Xie, L., An Evaluation of Blood Compatibility of Silver Nanoparticles. *Sci. Rep.* **2016**, *6*, 25518.
3. Sondi, I.; Salopek-Sondi, B., Silver Nanoparticles as Antimicrobial Agent: A Case Study on *E. coli* as a Model for Gram-Negative Bacteria. *J. Colloid Interface Sci.* **2004**, *275*, 177-182.
4. Zhang, Y.; Shareena Dasari, T. P.; Deng, H.; Yu, H., Antimicrobial Activity of Gold Nanoparticles and Ionic Gold. *J. Environ. Sci. Health, Part C* **2015**, *33*, 286-327.
5. Zhang, L.; Jiang, Y.; Ding, Y.; Povey, M.; York, D., Investigation into the Antibacterial Behaviour of Suspensions of ZnO Nanoparticles (ZnO Nanofluids). *J. Nanopart. Res.* **2007**, *9*, 479-489.
6. Liu, S.; Zeng, T. H.; Hofmann, M.; Burcombe, E.; Wei, J.; Jiang, R.; Kong, J.; Chen, Y., Antibacterial Activity of Graphite, Graphite Oxide, Graphene Oxide, and Reduced Graphene Oxide: Membrane and Oxidative Stress. *ACS Nano* **2011**, *5*, 6971-6980.
7. Ozkan, E.; Allan, E.; Parkin, I. P., White-Light-Activated Antibacterial Surfaces Generated by Synergy between Zinc Oxide Nanoparticles and Crystal Violet. *ACS Omega* **2018**, *3*, 3190-3199.
8. Brunet, L. n.; Lyon, D. Y.; Hotze, E. M.; Alvarez, P. J.; Wiesner, M. R., Comparative Photoactivity and Antibacterial Properties of C60 Fullerenes and Titanium Dioxide Nanoparticles. *Environ. Sci. Technol.* **2009**, *43*, 4355-4360.
9. Guo, M. Y.; Liu, F.; Leung, Y. H.; He, Y.; Ng, A. M. C.; Djurišić, A. B.; Li, H.; Shih, K.; Chan, W. K., Annealing-Induced Antibacterial Activity in TiO<sub>2</sub> under Ambient Light. *J. Phys. Chem. C* **2017**, *121*, 24060-24068.
10. Natalio, F.; André, R.; Hartog, A. F.; Stoll, B.; Jochum, K. P.; Wever, R.; Tremel, W., Vanadium Pentoxide Nanoparticles Mimic Vanadium Haloperoxidases and Thwart Biofilm Formation. *Nat. Nanotechnol.* **2012**, *7*, 530-535.
11. Pallavicini, P.; Dona, A.; Taglietti, A.; Minzioni, P.; Patrini, M.; Dacarro, G.; Chirico, G.; Sironi, L.; Bloise, N.; Visai, L., Self-Assembled Monolayers of Gold Nanostars: A Convenient Tool for Near-IR Photothermal Biofilm Eradication. *Chem. Commun.* **2014**, *50*, 1969-1971.
12. Teng, C. P.; Zhou, T.; Ye, E.; Liu, S.; Koh, L. D.; Low, M.; Loh, X. J.; Win, K. Y.; Zhang, L.; Han, M. Y., Effective Targeted Photothermal Ablation of Multidrug Resistant Bacteria and Their Biofilms with NIR-Absorbing Gold Nanocrosses. *Adv. Healthcare Mater.* **2016**, *5*, 2122-2130.
13. Raad, I.; Hanna, H.; Jiang, Y.; Dvorak, T.; Reitzel, R.; Chaiban, G.; Sherertz, R.; Hachem, R., Comparative Activities of Daptomycin, Linezolid, and Tigecycline against Catheter-Related Methicillin-Resistant *Staphylococcus* Bacteremic Isolates Embedded in Biofilm. *Antimicrob. Agents Chemother.* **2007**, *51*, 1656-1660.
14. Smith, K.; Perez, A.; Ramage, G.; Gemmell, C. G.; Lang, S., Comparison of Biofilm-Associated Cell Survival Following *In Vitro* Exposure of Meticillin-Resistant *Staphylococcus aureus* Biofilms to the Antibiotics Clindamycin, Daptomycin, Linezolid, Tigecycline and Vancomycin. *Int. J. Antimicrob. Agents* **2009**, *33*, 374-378.
15. Hengzhuang, W.; Wu, H.; Ciofu, O.; Song, Z.; Høiby, N., Pharmacokinetics/ Pharmacodynamics of Colistin and Imipenem on Mucoid and Nonmucoid *Pseudomonas aeruginosa* Biofilms. *Antimicrob. Agents Chemother.* **2011**, *55*, 4469-4474.



16. Bagge, N.; Schuster, M.; Hentzer, M.; Ciofu, O.; Givskov, M.; Greenberg, E. P.; Høiby, N., *Pseudomonas aeruginosa* Biofilms Exposed to Imipenem Exhibit Changes in Global Gene Expression and Beta-Lactamase and Alginate Production. *Antimicrob. Agents Chemother.* **2004**, *48*, 1175-1187.
17. Dean, C. R.; Visalli, M. A.; Projan, S. J.; Sum, P.-E.; Bradford, P. A., Efflux-Mediated Resistance to Tigecycline (Gar-936) in *Pseudomonas aeruginosa* PAO1. *Antimicrob. Agents Chemother.* **2003**, *47*, 972-978.
18. Deng, Y.; Sun, M.; Shaevitz, J. W., Direct Measurement of Cell Wall Stress Stiffening and Turgor Pressure in Live Bacterial Cells. *Phys. Rev. Lett.* **2011**, *107*, 158101.
19. Eaton, P.; Fernandes, J. C.; Pereira, E.; Pintado, M. E.; Xavier Malcata, F., Atomic Force Microscopy Study of the Antibacterial Effects of Chitosans on *Escherichia coli* and *Staphylococcus aureus*. *Ultramicroscopy* **2008**, *108*, 1128-1134.
20. Tuson, H. H.; Auer, G. K.; Renner, L. D.; Hasebe, M.; Tropini, C.; Salick, M.; Crone, W. C.; Gopinathan, A.; Huang, K. C.; Weibel, D. B., Measuring the Stiffness of Bacterial Cells from Growth Rates in Hydrogels of Tunable Elasticity. *Mol. Microbiol.* **2012**, *84*, 874-891.
21. Mathur, A. B.; Collinsworth, A. M.; Reichert, W. M.; Kraus, W. E.; Truskey, G. A., Endothelial, Cardiac Muscle and Skeletal Muscle Exhibit Different Viscous and Elastic Properties as Determined by Atomic Force Microscopy. *J. Biomech.* **2001**, *34*, 1545-1553.
22. Sato, M.; Nagayama, K.; Kataoka, N.; Sasaki, M.; Hane, K., Local Mechanical Properties Measured by Atomic Force Microscopy for Cultured Bovine Endothelial Cells Exposed to Shear Stress. *J. Biomech.* **2000**, *33*, 127-135.
23. Haga, H.; Sasaki, S.; Kawabata, K.; Ito, E.; Ushiki, T.; Sambongi, T., Elasticity Mapping of Living Fibroblasts by AFM and Immunofluorescence Observation of the Cytoskeleton. *Ultramicroscopy* **2000**, *82*, 253-258.
24. Simon, A.; Cohen-Bouhacina, T.; Porte, M.; Aime, J.; Amedee, J.; Bareille, R.; Baquey, C., Characterization of Dynamic Cellular Adhesion of Osteoblasts Using Atomic Force Microscopy. *Cytometry, Part A* **2003**, *54*, 36-47.
25. Lien, C. C.; Wu, M. C.; Ay, C., Study on the Young's Modulus of Red Blood Cells Using Atomic Force Microscope. *Appl. Mech. Mater.* **2014**, *627*, 197-201.